Supporting Information

Shim et al. 10.1073/pnas.1201882109

SI Text

SI Materials and Methods. ***Cell culture.*** BS-C-1 cells [CCL-26; American Type Culture Collection (ATCC)], an African green monkey kidney epithelial cell line, were maintained in a 5% CO_2 atmosphere at 37 °C in Eagle Modified Minimum Essential Medium (ATCC), supplemented with 10% fetal bovine serum (Invitrogen). Cells were passaged every 2–3 d and maintained for up to 20 passages. For imaging, cells were plated into eight-well chambered coverglasses (LabTek-II; Nalgene Nunc), previously cleaned with 1 M aqueous potassium hydroxide, at a density of 16,000–30,000 cells per well.

Hippocampal neuron culture was prepared largely as described previously (1). Briefly, hippocampi from embryonic 18 CFW mice (Charles River) were isolated and digested with trypsin, and neurons were plated onto poly-L-lysine/laminin-coated 12-mm coverslips in a plating medium. Three hours after plating, the coverslips with neurons were reversely placed into 24-well culture chambers with prepared glia. Five μM cytosine-β-D-arabinofuranoside was added to the culture to inhibit the growth of glial cells three days later. The neurons were fed twice a week with Neurobasal medium (Invitrogen) containing B-27 Supplement (Invitrogen) until use.

Live-cell labeling and imaging buffer. Live BS-C-1 cells and neurons were stained immediately before imaging. Approximately 36–48 h after plating, BS-C-1 cells were rinsed with Dulbecco's Modified Eagle Medium (DMEM) with high glucose (4.5 g/mL) and no phenol red (Invitrogen). Then, the cells were incubated in staining solution containing 10 μM DiI/DiD/DiR (Invitrogen), 0.2-1 μM MitoTracker Orange/Red/Deep Red (Invitrogen), 10–20 μM ER-Tracker Red (Invitrogen), or 1 μM LysoTracker Red (Invitrogen) in DMEM for 0.5–3 min. The stock solutions of all dyes were prepared by dissolving the dye powder in anhydrous DMSO at 25 mM for DiI/DiD/DiR and at 1 mM for other probes. For double-staining of mitochondria and the ER, cells were incubated in 0.2–0.5 μM MitoTracker Red in DMEM for 30 sec, washed two to three times with DMEM, and then incubated in 20 μM ER-Tracker Red in DMEM for 3 min. After staining, the cells were washed two to three times with DMEM and immediately used for imaging. Imaging medium was prepared with DMEM supplemented with 2% glucose, 6.7% of 1 M HEPES (pH 7.4), and an oxygen scavenging system (0.5 mg/mL glucose oxidase and 40 μg/mL catalase). BS-C-1 cells were imaged at room temperature.

Two to three weeks after plating, hippocampal neurons were rinsed with Neurobasal medium, incubated in DiI solution (approximately 10 μM in Neurobasal medium) at 37 °C for 1–2 min, and washed two to three times with Neurobasal medium. The neurons were allowed to recover in an incubator maintaining a 5% CO_2 atmosphere and 37 °C for at least 15 min before imaging. Labeled neurons were imaged in Neurobasal medium supplemented with 4% of 1 M HEPES (pH 7.4) and the oxygen scavenging system. While imaging, the neuron samples were placed in a stage incubator (Chamlide TC; LCI) set at 37 °C.

Fluorescence microscope. Most STORM experiments were performed on an Olympus IX-71 inverted optical microscope, except for DiR imaging. Here, we used three continuous wave lasers at wavelengths of 405 nm (CUBE 405-50C; Coherent), 561 nm (Sapphire 561-200; Coherent), and 657 nm (RCL-300-656; Crystalaser) controlled individually by mechanical shutters (Uniblitz LS6TS; Vincent Associates). The laser intensities were automatically controlled by an acousto-optic tunable filter (AOTF PCAOM NI VIS; Crystal Technology) for the 561- and 657-nm lines and by direct digital modulation of the laser power supply for the 405-nm line. All laser lines were combined and coupled into an optical fiber (Oz Optics), and the fiber output was collimated and focused at the back focal plane of a high numerical aperture (N.A.) oil immersion objective (100× UPlanSApo, NA1.40; Olympus). The dye molecules were imaged with excitation light of 561 nm for DiI, MitoTracker Orange/Red, and all BODIPY probes, or 657 nm for DiD and MitoTracker Deep Red. The excitation beams were reflected by longpass dichroic mirrors: ZT561RDC (Chroma) for 561 nm and T660LPXR (Chroma) for 657 nm. At the sample, the maximum laser intensity was 10 kW/cm^2 for the 561-nm line and 6 kW/cm^2 for the 657-nm line. Upon 561-nm or 657-nm illumination at high intensities, majorities of the probes were turned off to a dark state. Then, a low intensity of 405-nm illumination (typically 0–3 W/cm^2 at the sample) was used to activate the probes back to the fluorescence state. The 405-nm intensity was adjusted to maintain an approximately constant number of activated probes per frame and to compensate for the loss of fluorophores due to photobleaching. Except for Movie S6, the sample was continuously illuminated with the imaging and activation lasers. We typically imaged flat cell peripheries with approximately 1 μm thicknesses using a highly-oblique-incidence illumination geometry to reduce background. The fluorescence was collected by the same objective and imaged onto a back-illuminated EMCCD camera (iXon DU-860; Andor) running at 503 Hz with a 128 × 128 pixel region of interest (ROI) or at 909 Hz with a 64 × 128 pixels ROI. Fluorescence emission was filtered with the following filters: BLP01-561R (Semrock) for DiI and MitoTracker Orange; FF01-630/92 (Semrock) for MitoTracker Red, ER-Tracker Red and LysoTracker Red; ET705/72m (Chroma) for DiD and MitoTracker Deep Red.

For two-color imaging, both MitoTracker Red and ER-Tracker Red were excited using 561-nm light reflected by a longpass dichroic mirror (ZT561RDC; Chroma). The fluorescence emission was filtered by a longpass filter (BLP01-561R; Semrock), then split by a dicrhoic longpass (FF624-Di01; Semrock) mounted in a commercial image-splitting device (Dual-View; Photometrics). The two wavelength channels were further filtered by bandpass filters: ET595/50 (Chroma) in the short wavelength channel and FF01-630/92 (Semrock) in the long wavelength channel. Both channels were recorded by the EMCCD camera running at 503 Hz.

To stabilize the focus during data acquisition, an IR beam from an 830-nm fiber-coupled diode laser (LPS-830-FC; Thorlabs) was reflected from the coverglass-water interface and directed to a quadrant photodiode. The position readout of the quadrant photodiode provided a feedback to a piezo objective positioner (Nano-F100; MadCity Labs).

DiR was imaged on a nearly identical Olympus IX-71 microscope equipped with a 752-nm krypton laser (Innova 302C; Coherent), as described previously (2). The 752-nm line (approximately 1 kW/cm^2 at the sample) was reflected by a Q770DCXR dichroic (Chroma), and the fluorescence was filtered with an HQ800/60m emission filter (Chroma), and collected at a 33 Hz frame rate. The focus was locked by using a 975-nm IR laser (PL980P330J; Thorlabs), detecting the reflected beam from the coverglass-water interface with a quadrant photodiode and then compensating for the z-drift using a piezo stage (NZ100CE; Prior Scientific).

STORM image analysis. Two-dimensional live-cell STORM movies were analyzed using DAOSTORM software as previously described (3). DAOSTORM determines multiple molecular coordinates from overlapping images of individual molecules by iterating the following routine: (*i*) From the original image, candidate molecules were identified and fit with a Gaussian function of a fixed width; (*ii*) The residual image was inspected to identify extra molecules; (*iii*) Multiple overlapping Gaussian functions were then used to fit the original image with the updated list of candidate molecules including the extra molecules from the residual image. Three-dimensional STORM movies were analyzed using a custom-written software in C++ that fits individual molecular images to an elliptical Gaussian function with variable widths. The centroid positions of the Gaussian were used to determine the lateral coordinates of the molecules and the Gaussian widths were used to determine the axial positions of the molecules as described previously (4). Sample drift was negligible in live-cell images because of the relatively short imaging time. For fixed-cell images, both lateral and axial drifts were measured and corrected by image correlation as described previously (4). Finally, STORM images were rendered with each localization plotted as a 2D Gaussian whose width is weighted by the inverse square root of the number of detected photons. Background signals coming from cellular autofluorescence and nonspecifically bound probes appear as scattered localizations at low local densities, and were removed by a local density filter as previously described (5).

Localization precision and Nyquist resolution. To quantify the spatial resolution achieved with each of the membrane probes, we experimentally determined both the localization precisions and the Nyquist resolution limits based on the localization densities. For measuring localization precisions, BS-C-1 cells were labeled with fixable membrane probes (CM-DiI, MitoTracker Red, ER-Tracker Red and LysoTracker Red; Invitrogen) at a labeling density low enough to distinguish individual probes in the STORM images. The labeled cells were fixed with 3% PFA and 0.1% glutaldehyde for 10–15 mins at 37 °C to immobilize the probes. The fixed cells were imaged with the same imaging conditions used in live-cell experiments. The fixed probes typically emit 10–20% fewer photons than the corresponding probes in living cells and hence slightly underestimate the localization precision. The distributions of multiple localizations obtained from individual fixed probes were used to determine the localization precisions.

To determine the Nyquist resolution limits based on localization densities, the STORM images were thresholded by Otsu's method (6) to measure the area of the structure of interest and to determine the number of localizations within the area of interest. Then, the Nyquist resolution was computed as $2/[(\text{number of localizations})/(\text{area})]^{1/2}$ (7).

Characterization of photoswitching properties. The on-off duty cycle values and the total number of switching cycles included in Table S1 were measured in fixed BS-C-1 cells sparsely labeled with fixable membrane probes as in the case of measuring localization accuracy. The fixed samples were imaged for more than 20 min with the 561-nm imaging laser and no 405-nm activation laser. After localization analysis, we linked nearby localizations in subsequent frames as a single switching event and obtained number of cycles and duty cycles in ways similar to those described previously (2). The on-off duty cycle was defined as the sum of on-times divided by the entire trajectory length until bleaching.

On-off contrast ratios were measured in live cells. Conventional fluorescence images of the organelles were obtained before and immediately after a strong 561-nm illumination was used to switch off the probes. To measure the bulk fluorescence intensities of the organelles in the bright and the dark state, organelles were identified from images before strong illumination. Areas outside the identified organelles were used to measure the background intensity. Because of the rapid fluorescence recovery (due to the diffusion of fluorescent probes into the imaging region and reactivation of switched off probes), the fluorescence intensity of the dark state of these probes may be overestimated. Hence, the contrast ratios were lower bound values.

Particle tracking. After localizing the probes, localizations in consecutive frames within a radius of 2 pixels (312 nm) were assumed to be from the same probe and linked to produce trajectories. Under our experimental conditions in Fig. 3, the mean distance between neighboring activated molecules was typically approximately 3 μm, which ensured sufficiently low density of molecules to prevent linking different molecules into the same trajectory. All subsequent analysis was carried out using a custom-written MATLAB code. The diffusion coefficients were obtained by calculating the mean-squared displacements (MSD) for all trajectories containing at least 15 steps, and then fitting MSD for the first four time lags ($0 < \Delta t \leq 8$ msec) with a linear fit, as is commonly used in standard single-particle-tracking analysis (8). This procedure was also used previously for high-density particle-tracking analysis using photoactivatable proteins (9).

Width measurements of various tubule structures. The widths of spine necks, intermitochondrial tubules, and ER tubules in Figs. 2*A*, 4*B* and 5*C* were measured from STORM images by fitting transverse profiles of localization with Gaussians. To obtain the transverse profiles, regions of interests were chosen with boxes of various widths (all >200 nm) that enclose roughly straight tubes with constant widths. The localizations within the box were counted and binned with 20-nm intervals. The histograms were fit with Gaussians and full-width-at-half-maximum (FWHM) values were reported. The same method was used throughout the paper except for Fig. S3 (see the figure caption for the specific method used in this figure).

Color assignment for two-color images. Because the spectral separation of the ER dye (ER-Tracker Red) and the mitochondrial dye (MitoTracker Red) is only 16 nm, we used a ratiometric method to assign the colors of images of these dyes (10–13). Each probe was detected in two channels: a short wavelength channel and long wavelength channel separated by a 624-nm longpass dichroic mirror. After identifying peaks corresponding to individual molecules in each channel, the molecular coordinates in the long wavelength channel were overlaid on the short wavelength channel by using the transformation map obtained from calibration images of 100-nm fluorescent beads (Tetraspeck; Invitrogen). Peaks in the two channels within a radius of 0.5 pixels (78 nm) were paired and assumed to belong to the same molecule. The photon numbers detected in the two channels (n_{long}, n_{short}) were determined for individual molecules and used to determine whether the molecule was the ER dye or the mitochondrial dye.

For calibration purposes, we first determined the distributions of (n_{long}, n_{short}) for samples singly stained with either the ER dye or the mitochondrial dye (Fig. S5). Two types of single-color samples were imaged: (*i*) the ER dye or the mitochondrial dye adsorbed on coverslips; (*ii*) live cells labeled with either the ER dye or the mitochondrial dye. For probes adsorbed on coverslips, the detected photons from a single probe formed a distribution along a characteristic ratio $n_{\text{long}}/n_{\text{short}}$ with expected spread due to the finite emission bandwidths of the two dyes and the shot noise (Fig. S5*A*). In live cells, the $n_{\text{long}}/n_{\text{short}}$ ratio of the mitochondrial dyes was largely unchanged, but the ER dyes split into two populations with blue- and red-shifted spectra (Fig. S5*B*). Because the ER dye binds to potassium channels enriched in ER, the two spectrally distinct populations may indicate two different states of the dye-protein complex.

We assigned individual localizations in the two-color images to the ER and mitochondrial color channels using a statistical approach as previously reported (11). Briefly, we estimated maximum likelihood of probe identities based on the $(n_{\text{long}}, n_{\text{short}})$ values of individual localizations using calibration data sets derived from live cells singly labeled with the ER or mitochondrial probes. From the two calibration data sets, 2D frequency histograms of $(n_{\text{long}}, n_{\text{short}})$ $[p_{\text{ER}}(n_{\text{long}}, n_{\text{short}})$ and $p_{\text{MT}}(n_{\text{long}}, n_{\text{short}})$ (MT: mitochondria)] were obtained with bins of 50 photons. The probe identity of any given $(n_{\text{long}}, n_{\text{short}})$ was determined with a maximum-likelihood estimator: the estimated color, $T(n_{\text{long}}, n_{\text{short}})$ was simply chosen as the probe with larger probability; i.e.,

$$T(n_{\text{long}}, n_{\text{short}}) = \begin{cases} \text{ER} & \text{if } p_{\text{ER}} > p_{\text{MT}}, \\ \text{MT} & \text{if } p_{\text{ER}} < p_{\text{MT}}. \end{cases} \quad \textbf{[S1]}$$

Then, the confidence level C was calculated as follows:

$$C = \begin{cases} \frac{p_{\text{ER}}}{p_{\text{ER}}+p_{\text{MT}}} & \text{if } p_{\text{ER}} > p_{\text{MT}}, \\ \frac{p_{\text{MT}}}{p_{\text{ER}}+p_{\text{MT}}} & \text{if } p_{\text{ER}} < p_{\text{MT}}. \end{cases} \quad \textbf{[S2]}$$

A threshold confidence level of 0.70 was used to define regions of specific color assignment shown in Fig. S5*C*. We also excluded regions where the calibration data contained less than four events within the bin. This method discarded 20–40% of total localizations as uncertain points. The color cross-talk from the ER channel to the mitochondria channel was determined as 16%, while the cross-talk from the mitochondria channel to the ER channel was 28%.

1. Kaech S, Banker G (2006) Culturing hippocampal neurons. *Nat Protocols* 1:2406–2415.
2. Dempsey GT, Vaughan JC, Chen KH, Bates M, Zhuang XW (2011) Evaluation of fluorophores for optimal performance in localization-based super-resolution imaging. *Nat Methods* 8:1027–1036.
3. Holden SJ, Uphoff S, Kapanidis AN (2011) DAOSTORM: An algorithm for high-density super-resolution microscopy. *Nat Methods* 8:279–280.
4. Huang B, Wang W, Bates M, Zhuang X (2008) Three-dimensional super-resolution imaging by stochastic optical reconstruction microscopy. *Science* 319:810–813.
5. Jones SA, Shim SH, He J, Zhuang X (2011) Fast, three-dimensional super-resolution imaging of live cells. *Nat Methods* 8:499–508.
6. Sezgin M, Sankur B (2004) Survey over image thresholding techniques and quantitative performance evaluation. *J Electron Imaging* 13:146–165.
7. Shroff H, Galbraith CG, Galbraith JA, Betzig E (2008) Live-cell photoactivated localization microscopy of nanoscale adhesion dynamics. *Nat Methods* 5:417–423.
8. Saxton MJ (1997) Single-particle tracking: The distribution of diffusion coefficients. *Biophys J* 72:1744–1753.
9. Manley S, et al. (2008) High-density mapping of single-molecule trajectories with photoactivated localization microscopy. *Nat Methods* 5:155–157.
10. Schonle A, Hell SW (2007) Fluorescence nanoscopy goes multicolor. *Nat Biotechnol* 25:1234–1235.
11. Bossi M, et al. (2008) Multicolor far-field fluorescence nanoscopy through isolated detection of distinct molecular species. *Nano Lett* 8:2463–2468.
12. Testa I, et al. (2010) Multicolor fluorescence nanoscopy in fixed and living cells by exciting conventional fluorophores with a single wavelength. *Biophys J* 99:2686–2694.
13. Gunewardene MS, et al. (2011) Superresolution imaging of multiple fluorescent proteins with highly overlapping emission spectra in living cells. *Biophys J* 101:1522–1528.

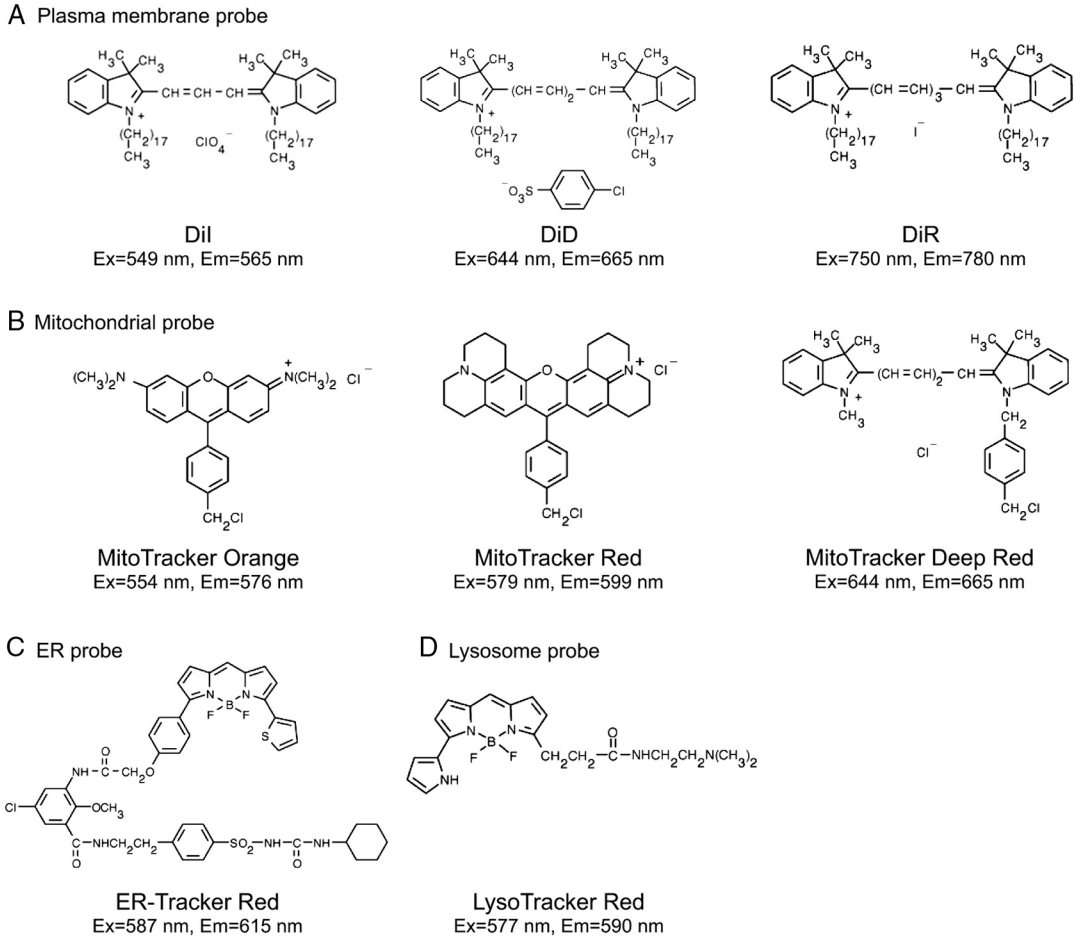

Fig. S1. Chemical structures of the eight photoswitchable membrane probes, each specific for the plasma membrane (*A*), mitochondria (*B*), the ER (*C*) or lysosomes (*D*). For each probe, wavelengths at its excitation and emission maximum are displayed as "Ex" and "Em", respectively.

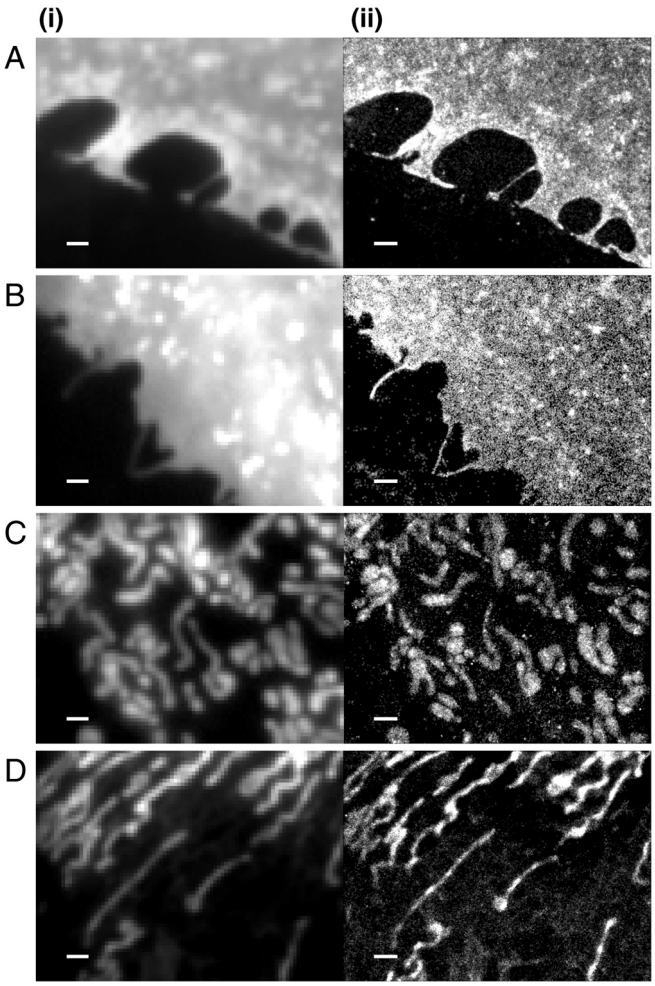

Fig. S2. STORM images of live BS-C-1 cells labeled with DiD, DiR, MitoTracker Orange, or MitoTracker Deep Red. (*A* and *B*) Conventional (*Left*) and STORM (*Right*) images of the plasma membrane stained with DiD (*A*) and DiR (*B*). (*C* and *D*) Conventional (*Left*) and STORM (*Right*) images of mitochondria labeled with MitoTracker Orange (*C*) and MitoTracker Deep Red (*D*). The conventional fluorescence images were taken prior to STORM imaging with a low excitation intensity that did not switch off the probes appreciably. Scale bars, 1 μm.

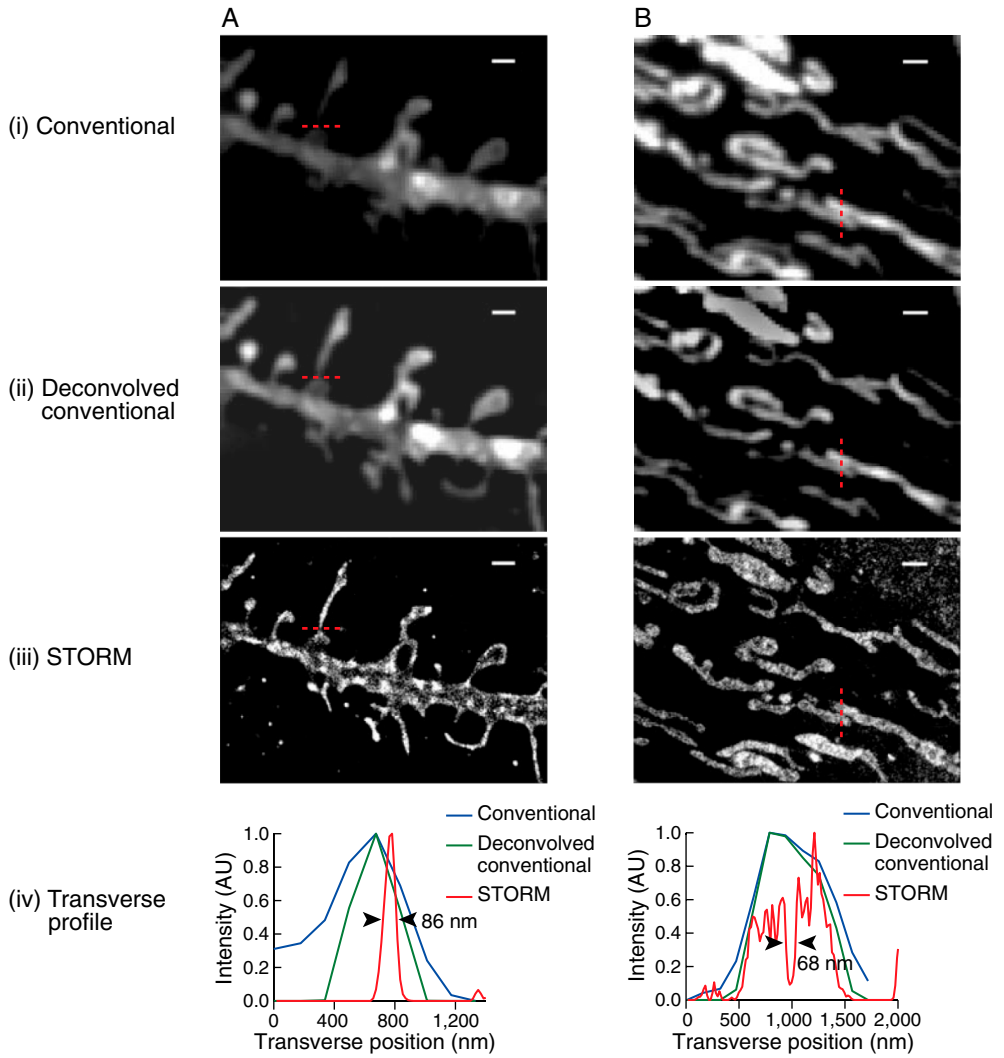

Fig. S3. Comparison of conventional (*i*), deconvolved conventional (*ii*), and STORM (*iii*) images of the plasma membrane of the hippocampal neuron (*A*) and mitochondria in the BS-C-1 cell (*B*) in Fig. 2 *A* and *B* in the main text. The profiles (*iv*) along the red dash line show enhanced resolution of the STORM images (red lines) as compared to that of the conventional (blue lines) and deconvolved conventional (green lines) images; in particular, the approximately 90-nm-thick neck of a dendritic protrusion in *A* and the approximately 70-nm-wide gap between adjacent mitochondria in *B* were blurred in both of the conventional images, but clearly resolved in the STORM images. STORM images were collected immediately after acquiring the conventional fluorescence images. Due to the time lapse between the conventional and STORM images, the structures could have moved slightly. The deconvolved images were obtained from the conventional image using a plug-in to ImageJ (http://www.optinav.com/Iterative-Deconvolution.htm) and the point-spread-function obtained from single-molecule images of DiI or MitoTracker Red. The intensity profiles from the conventional and deconvolved images present intensity values from individual pixels where the red dash line is placed. The STORM profiles were generated by integrating the intensity of the STORM images within a 70-nm-wide box. These profiles, binned with 40-nm intervals, were then fitted with Gaussians to determine the width in FWHM, as indicated in the plots. Scale bars, 1 μm.

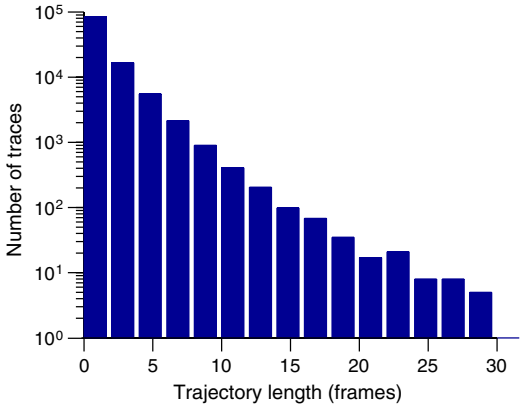

Fig. S4. Length distribution of all trajectories of DiI molecules detected in the live neuron in Fig. 3. Note that the subsequent analysis used only long trajectories with more than 15 steps to obtain diffusion coefficients with reasonable accuracy.

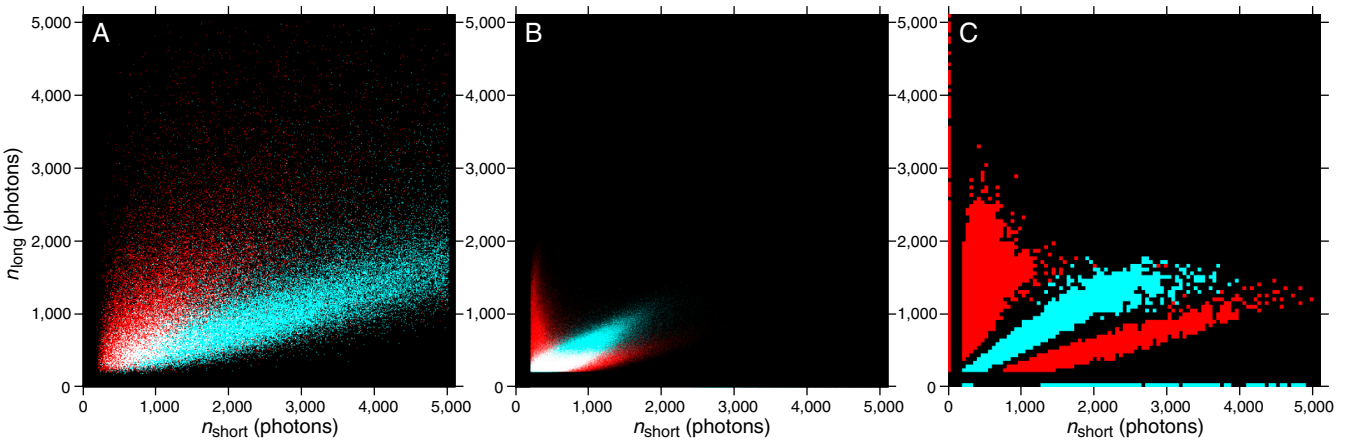

Fig. S5. Calibration measurements of MitoTracker Red (cyan) and ER-Tracker Red (red) for color assignment in two-color imaging. (*A*) Photon number distribution in the two channels (long and short wavelengths) measured for MitoTracker Red (cyan) and ER-Tracker Red (red) adsorbed on coverslips. All events with photon numbers above 5000 were excluded. Photon numbers below 150 were undetected due to an intensity threshold used for peak identification. (*B*) Photon number distribution measured for live BS-C-1 cells singly labeled with either MitoTracker Red (cyan) or ER-Tracker Red (red). Here n_{long} and n_{short} indicate the number of photons detected per camera frame. Each activation event typically lasted longer than one camera frame at ~500 Hz. We note that n_{long} and n_{short} shown panels *A* appear bigger than those shown in *B* because different camera frame rates were used for these two measurements (150 Hz for *A*, 503 Hz for *B*). The brightness of the probes in live cell was actually similar to those adsorbed on coverslips. (*C*) Regions of specific color assignment defined by a threshold confidence level of 0.70 for MitoTracker Red (cyan) and ER-Tracker Red (red).

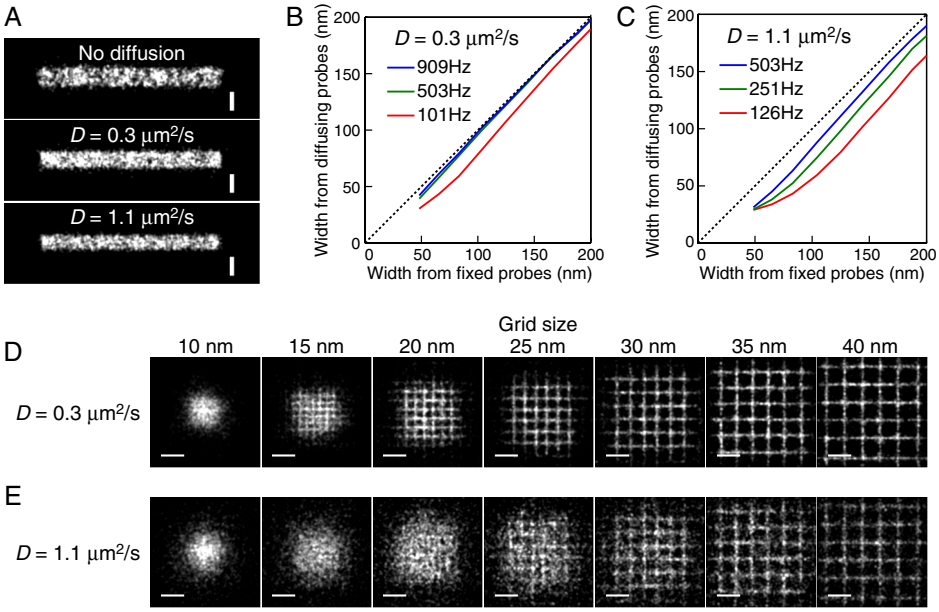

Fig. S6. Effects of probe diffusion on STORM images. (*A*) Simulated STORM images of a tube structure with 100-nm actual width probed with fixed fluorophores (*Top*) and diffusing fluorophores (*Middle* and *Bottom*). The diffusion coefficient, *D*, was chosen to be equal to those of MitoTracker Red (*Middle*) and DiI (*Bottom*). For each camera frame at 503 Hz, a diffusion trace with 500 steps (4 μs each step) was generated within the boundary of the tube structure based on these diffusion coefficients. Then, a point-spread-function (PSF) with realistic photon numbers based on experimental values was translated along the trajectory to generate a molecular image. Noise (also set based on experimental values) was then added to the image. Molecular images of 2,000 probes were generated this way and fitted to 2D Gaussians to determine the molecular localizations, as plotted in each panel here. (*B*) The measured widths derived from simulated STORM images for tube structures with varying actual widths. The x-axis of the plot represents the measured width of the tubes probed with fixed fluorophores and the y-axis represents the corresponding values derived from diffusing fluorophores. The diffusion coefficient, *D*, of the diffusing probes was set to be equal to that of MitoTracker Red ($D = 0.3\ \mu m^2/s$). The simulated camera frame rates were 909 Hz (blue), 503 Hz (green), or 101 Hz (red). Specifically, for any given frame rate and actual tube width, STORM images were generated for $D = 0$ and $D = 0.3\ \mu m^2/s$ as in *A*. Then, from the transverse profiles of localizations, the widths of the tube images (in FWHM) were measured by fitting the localization profiles with Gaussians. (*C*) Same as in *B* except that the diffusion coefficient of the diffusing probes was set to be equal to that of DiI ($D = 1.1\ \mu m^2/s$). The simulated camera frame rates were 503 Hz (blue), 251 Hz (green), or 126 Hz (red). Note that the measured widths of the tube structures with diffusing probes converges to approximately 30 nm, which is equal to the localization accuracy of the probes. (*D* and *E*) Simulated STORM images of grid structures with grid sizes ranging from 10–40 nm for diffusing fluorophores with diffusion coefficient $D = 0.3\ \mu m^2/s$ (*D*) and $D = 1.1\ \mu m^2/s$ (*E*). The images were simulated considering the realistic photon numbers detected from the probes and the realistic noise at camera frame rate of 503 Hz in a way similar to that described in *A*, except that the confining structure is changed from tubes to grids. Scale bars, 100 nm in (*A*) and 50 nm in (*D* and *E*).

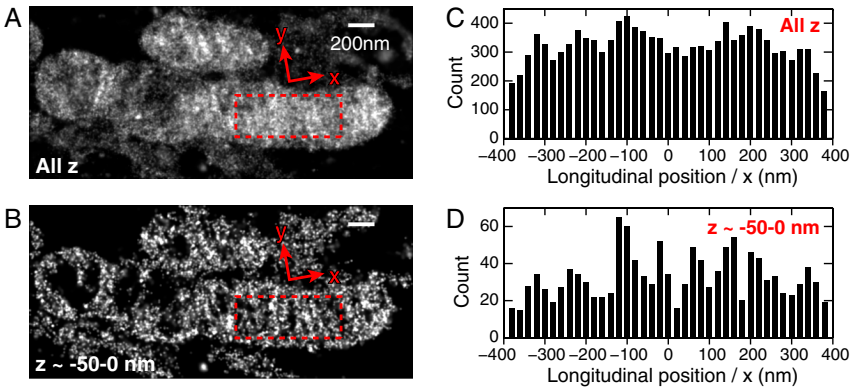

Fig. S7. 3D STORM images of mitochondria in a fixed BS-C-1 cell. The cell was labeled with MitoTracker Red while alive and subsequently fixed. (*A* and *B*) A 2D projection image of mitochondria (*A*) and its corresponding z cross-section image with $z \sim -50$–0 nm (*B*). The focal plane is at $z = 0$. (*C*) Longitudinal profiles of localizations of the red-boxed region in *A*. (*D*) Localization profiles of the red boxed region in *B*. To generate the localization profiles, the molecular coordinates within the boxed region were projected to an axis perpendicular to most of the cristae in the region, indicated as "*x*" in *A* and *B*. Scale bars, 200 nm.

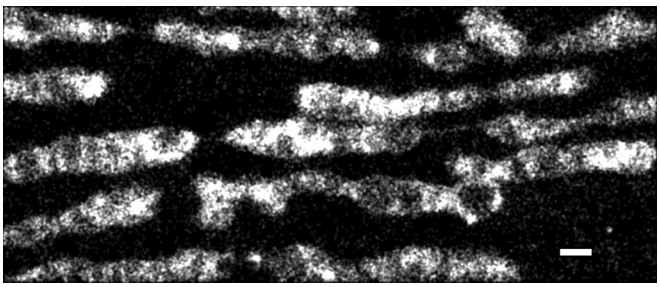

Movie S1. STORM movie of mitochondria labeled with MitoTracker Red in a live BS-C-1 cell. The same field of view as shown in Fig. 4*C*. Two-sec snapshots are displayed at 5× real time. Scale bar, 500 nm.

Movie S1

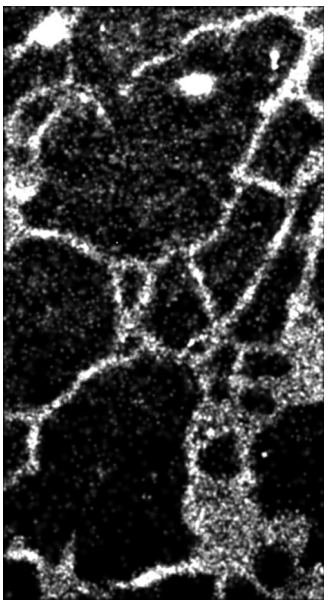

Movie S2. STORM movie of the ER labeled with ER-Tracker Red in a live BS-C-1 cell. The same field of view as shown in Fig. 5*A*. The movie runs in real time with 10-sec snapshots.

Movie S2 (MOV)

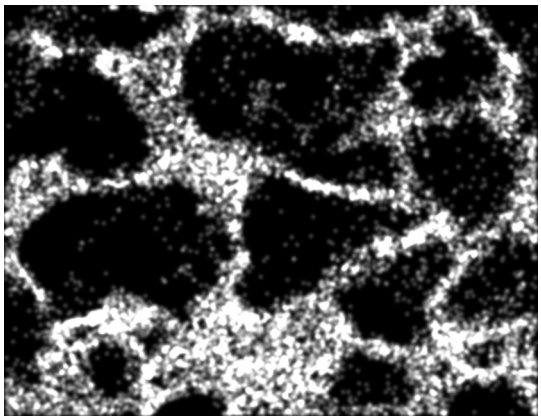

Movie S3. STORM movie of the ER network labeled with ER-Tracker Red in a live BS-C-1 cell. The same field of view as shown in Fig. 5*D*. The movie runs in real time with 2-sec snapshots.
Movie S3 (MOV)

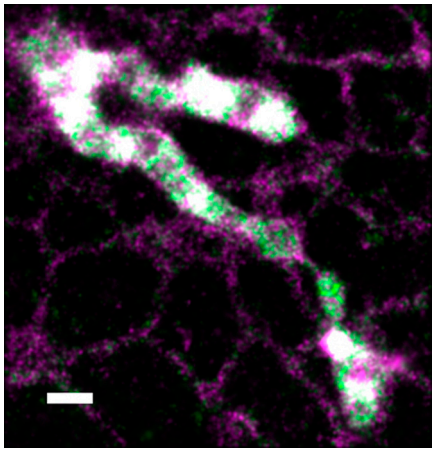

Movie S4. Two-color STORM movie of mitochondria (green) and the ER (magenta) in a live BS-C-1 cell. The field of view here is the same as that shown in Fig. 6. The movie runs at 5× real time with 10-sec snapshots. Scale bar, 500 nm.
Movie S4 (MOV)

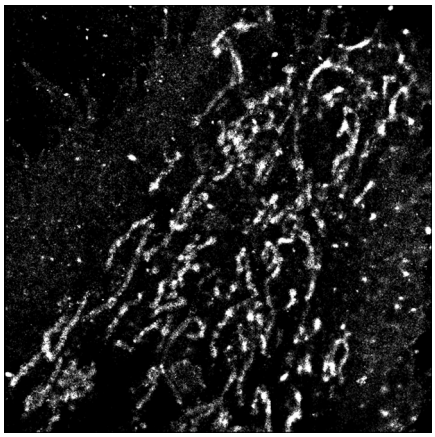

Movie S5. Five-min-long STORM movie of mitochondria labeled with MitoTracker Red in a live BS-C-1 cell imaged with continuous illumination. The mitochondrial morphology largely remained unperturbed within the first minute. Then, the elongated mitochondria slowly turned into spherical or disk-like shapes, indicating stress on mitochondria. The video runs at 10× real time with 5-s snapshots.
Movie S5 (MOV)

Movie S6. Twelve-min-long STORM movie of mitochondria labeled with MitoTracker Red in a live BS-C-1 cell imaged with strobed illumination. The 405 and 561-nm illumination was turned on for two frames followed by six frames of dark period with no light. The excitation sequence effectively reduces the amount of light exposure to the cell by 4 fold. The mitochondrial morphologies remained largely unchanged throughout the movie. The video runs at 10× real time with 20-sec snapshots.
Movie S6 (MOV)

Table S1. Photoswitching properties of the four representative membrane probes used in this study

Probe	Photon number per frame*	Localization accuracy in SD (FWHM)*	Number of switching cycles	On-off duty cycle†	Contrast ratio‡
DiI	720	17 (40) nm	27	0.0006	≥1000
MitoTracker Red	790	13 (30) nm	74	0.0017	≥1000
ER-Tracker Red	820	15 (35) nm	28	0.0003	≥1000
LysoTracker Red	820	13 (30) nm	26	0.0003	≥1000

*We report these numbers per frame even though single switching events typically last a couple frames on average. Because these probes can diffuse on the membrane, combining photons from multiple consecutive frames could effectively reduce the localization precision due to motion blurring.

†The on-off duty cycle is defined as the fraction of time that the molecules spend in their on-state before photobleaching.

‡The contrast ratio is defined as the ratio of fluorescence intensities between the fluorescent state and the dark state.